Available online at www.sciencedirect.com
ScienceDirect
Journal of Photochemistry and Photobiology A: Chemistry 188 (2007) 218–225
Journal of Photochemistry and Photobiology A:Chemistry
www.elsevier.com/locate/jphotochem

Effects of synergetic ligands on structure and fluorescence properties of Langmuir and Langmuir–Blodgett films containing $Eu(TTA)_3nL$

Si Wu, Pingsheng He, Junbo Guan, Biao Chen, Yanhua Luo, Qing Yan, Qijin Zhang *

Department of Polymer Science and Engineering, University of Science and Technology of China, Hefei, Anhui 230026, PR China

Received 5 September 2006; received in revised form 9 November 2006; accepted 12 December 2006
Available online 16 December 2006

Abstract

Effects of synergetic ligands of the europium complexes $Eu(TTA)_3nL$ (Eu denotes the central ion Eu(III), TTA denotes the β-diketone ligand α-thenoyltrifluoroacetone, L denotes the synergetic ligands triophenylphosphine oxide, 1,10-phenanthroline, 2,2′-bipy and H_2O, respectively) on fluorescence properties and supermolecular structures of Langmuir and Langmuir–Blodgett films were studied. Experiments on the Langmuir trough showed that different supermolecular structures were formed for each complex with different synergetic ligands, in which aggregate structure was found at the air/subphase interface for $Eu(TTA)_3Phen$ and multilayer structure for the other three complexes. This result is accordance with the *R* values calculated in terms of their fluorescence spectra. Fluorescence enhancement was found to be in an order of the relative emission intensity of the fluorescent LB films: $I(Eu(TTA)_3(TPPO)_2) > I(Eu(TTA)_3Phen) > I(Eu(TTA)_3Bipy) > I(Eu(TTA)_3{\cdot}2H_2O)$. Detailed analysis on the LB film containing $Eu(TTA)_3(TPPO)_2$ revealed that the LB film containing $Eu(TTA)_3(TPPO)_2$ not only have the strongest red light emit, the best monochromacity, good miscibility with arachidic acid (AA), but also have condensed structure, controllable nanometer-scale thickness and vertical uniformity.

Keywords: Fluorescence; Rare earth complex; Synergetic ligand; Langmuir–Blodgett film

1. Introduction

Because of their numerous applications [1–4], rare earth complexes have attracted more and more attentions in areas of chemistry, physics, biology and material science. It is found that supermolecular structure plays an important role in properties and applications of rare earth complexes containing materials [5].

In our previous work [6–9], the fluorescence properties of rare earth complexes and their applications in optical fiber, optical fiber amplifier and three-dimensional multilayered optical memory materials were studied. It is also found that $Eu(TTA)_3nL$ (TTA = thenoyltrifluoroacetonatone; L = TPPO from tribenylphosphine oxide, Phen from 1,10-phenanthroline, Dipy from 2,2-bipy and TOPO from trioctylphosphine, respectively) can be easily dispersed into poly(methyl methacrylate) (PMMA) to form solid solutions which are of good thermal stability and promising to be candidates for laser materials in future applications [10]. $Eu(TTA)_3{\cdot}2H_2O$ was found to form J-aggregate on the surface of silver nanoparticles, high fluorescence properties of such nanoparticles were resulted from the efficiently local field enhancement due to surface plasmon resonance (SPR) excitations [11]. These results reveal that not only ligands but also matrixes will affect the luminescent properties and applications of rare earth complexes. In this paper, Langmuir–Blodgett technique is used to fabricate ultrathin film materials containing $Eu(TTA)_3nL$ to further investigate the relationship between structure and fluorescent properties under such a circumstance, and based on the rare earth containing ultrathin films can be developed.

Langmuir–Blodgett technique is a very powerful tool to fabricate ultrathin films with highly ordered structures [12,13] and controllable molecular array for efficient energy and electron transfer [14,15]. There are generally three methods to fabricate the functional LB films. Many workers employed metal salts in the aqueous subphase to incorporate groups into LB films [16–21]. The metal ions were adsorbed onto the fatty acid film from the subphase by a stochastic process. Therefore, it is

* Corresponding author. Tel.: +86 551 3601704; fax: +86 551 3601704.
E-mail address: zqjm@ustc.edu.cn (Q. Zhang).

1010-6030/$ – see front matter © 2007 Elsevier B.V. All rights reserved.
doi:10.1016/j.jphotochem.2006.12.020

hard to control the concentration of the functional molecules and the functions of the LB films due to the stochastic process. Chemical modification is another method to obtain amphiphilic functional molecules to fabricate LB films. This method needs a complex chemical synthesis that limits the applications of some functional materials and there are some problems when the monolayer is transferred onto the substrate. Wang et al. tried to use this method to fabricate high ordered europium complex LB films [22]. They synthesized a rare earth complex with a long chain on the synergetic ligand. The complex could not be efficiently transferred onto the substrate at lower surface pressure and showed a quenched emission when transferred at higher surface pressure. To conquer the defects of the two methods mentioned above, the third method was used [23], in which the mixture of classical film-forming molecules (for example, AA) and functional metal complexes were used to fabricate the functional LB films.

Due to the poor absorption, rare earth ions are not used directly but to form complexes with organic ligands that absorb light and transfer the energy to ions. In addition, synergetic ligands, which do not transfer light energy to ions, are usually adopted to expel adsorbed water from the first coordination sphere because water molecules can cause radiationless deactivation. Recently, synergetic ligands were used to control the supermolecular structure of rare earth complexes [24] and grafted the complex onto the host matrix to form homogeneous stable functional materials [25]. Although using LB technique can also control the supermolecular structure and get a homogeneous film material, there is no work about how synergetic ligands affect the properties of LB films to our knowledge. In this paper, the work is presented on effect of synergetic ligands on supermolecular structures and fluorescence properties of LB films containing $Eu(TTA)_3nL$.

2. Experiment

2.1. Materials

Synthesis of rare earth complexes was described in our previous work published elsewhere [10], and the structures of the rare earth complexes are shown in Fig. 1. The rare earth complexes studied in this paper are used as functional molecules. Arachidic acid ($CH_3(CH_2)_{18}COOH$, AA, spectrum purity) is a Fluka product and is used without further purification. AA is used to control the thickness of LB films at nanometer-scale.

AA and the complexes were all dissolved into the chloroform separately to obtain solutions with the same concentration of 5×10^{-4} mol/L. Other chemical agents were all A.R. grade.

2.2. Subphases

Double distilled water (doubly distilled and purified by a quartz subboiling ultrapurified distiller, pH 5.8) was used in experiments. The composite subphase was obtained according to Ref. [26]. First, excess amount of complex, and corresponding TTA and L (L is the synergetic ligands, L = Phen, Bipy, TPPO and water) were put into the double distilled water (For example, if the π–A curve of mixed $Eu(TTA)_3Phen$ and AA was measured, $Eu(TTA)_3Phen$, TTA and Phen should be put into the double distilled water to obtain the subphase); then shaking fiercely and leaving the solution overnight; finally filtering the solution and using the filtrate as the composite subphase. In this way, TTA, the synergetic ligand as well as the complex were all saturated in the composite subphase.

2.3. Monolayer measurements and deposition procedure

All of monolayer measurements and LB films deposition were carried out on a home-made computer-controlled Langmuir trough (40 cm × 15 cm) with Wilhelmy Pt-plates placed in a dust-free box at 19 ± 1 °C. The monolayer-forming solution was spread by a micro-injector on the subphase surface of the Langmuir trough. The spread monolayer was compressed with a barrier at a constant rate of 8 mm/min after 20 min for solvent evaporation. The average molecular area of the mixed monolayer could be calculated (dividing total occupied area by the number of molecules of arachidic acid plus the number of the rare earth complexes). The changes of surface pressure

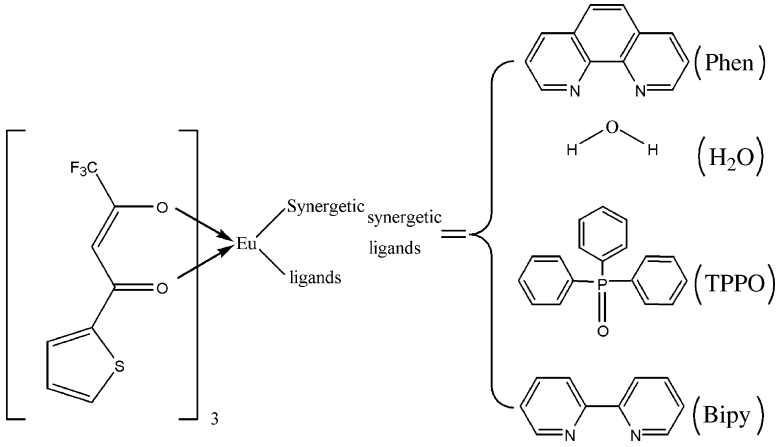

Fig. 1. Molecular structures of $Eu(TTA)_3Phen$, $Eu(TTA)_3 \cdot 2H_2O$, $Eu(TTA)_3(TPPO)_2$ and $Eu(TTA)_3Bipy$.

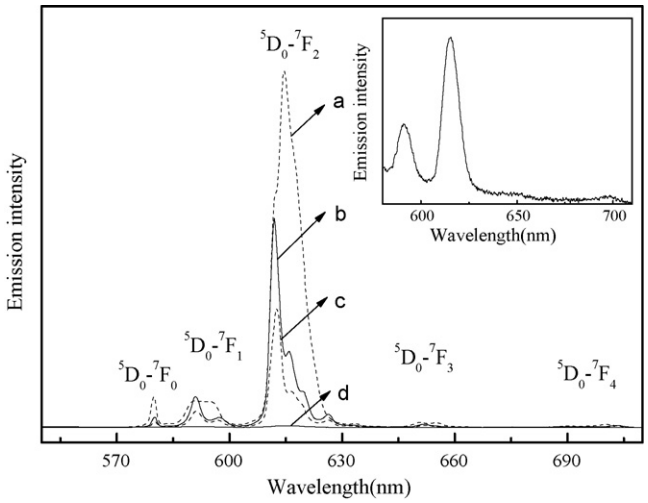

Fig. 2. Fluorescence spectra of 16 layers of AA/Eu(TTA)$_3$nL = 1/1 LB films. (a) AA/Eu(TTA)$_3$(TPPO)$_2$, (b) AA/Eu(TTA)$_3$Phen, (c) AA/Eu(TTA)$_3$Bipy and (d) AA/Eu(TTA)$_3$·2H$_2$O. The inset is the enlargement of fluorescence spectra of AA/Eu(TTA)$_3$·2H$_2$O.

and average molecular area of the mixed monolayer were both recorded by a computer. Therefore, π–A isotherm curve of the mixed monolayer could be obtained. LB films were deposited at a constant surface pressure of 30 mN/m and a deposition speed of 2 mm/min, containing AA with the molar ratio of 50%. The substrates for LB films deposition were hydrophobic quartz slides for UV–vis spectrum measurements and cover-glass slides for the other measurements.

2.4. Spectroscopy

A Shimadzu RF-5301PC Fluorescence Spectrophotometer was used to measure fluorescence spectra of the LB films. The excitation spectra were measured before the fluorescence spectra and the best excitation wavelengths were found (the best excitation wavelengths for exciting AA/Eu(TTA)$_3$nL LB films were: 345 nm for AA/Eu(TTA)$_3$Phen, 353 nm for AA/Eu(TTA)$_3$Bipy, 356 nm for AA/Eu(TTA)$_3$(TPPO)$_2$ and 357 nm for AA/(Eu(TTA)$_3$·2H$_2$O), respectively). The small angle X-ray diffraction profile was recorded on a PHILIPS X' PERT PRO X-ray diffract meter using Cu Kα line (λ = 0.15418 nm) with DS = 1°, SS = (1/8)°, RS = 0.1 mm. UV–vis absorption spectra were measured with a 756PC Spectrophotometer (Shanghai).

3. Results and discussion

3.1. Fluorescence properties

The fluorescence spectra of the AA/Eu(TTA)$_3$nL (AA:Eu = 1:1) LB films is shown in Fig. 2. Five Eu^{3+} characteristic emission peaks which are assignable to $^5D_0 \rightarrow {}^7F_j$ (j = 0–4) can be observed. In addition, the emission intensity of LB films containing Eu(TTA)$_3$(TPPO)$_2$ is the strongest; the emission intensity of LB films containing Eu(TTA)$_3$·2H$_2$O is the weakest. This result is accordance with that derived from the vibrational energy. The vibration of the P=O is at around 1125 cm^{-1}, C=N is at around 1601 cm^{-1}, and O–H is at around 3400 cm^{-1}. The bigger the wave number is, the more vibrational energy will be consumed, and the efficient energy, which is used to creating fluorescence, will be reduced [10]. The energy absorption and transfer process of rare earth complex is shown in Fig. 3a. When the β-diketone ligand TTA absorbed the UV light, it will be at excited state. The energy of the excited TTA will be transferred to the central ion Eu^{3+} as well as the synergetic ligand at a lower level. By the resonance and inductive effects, the synergetic ligands can change the electron density at the keto-enol oxygen metal-to-oxygen bond and the ease of transmission of excitation energy through these bonds. As a result, these factors may affect the emission process of Eu^{3+} and thus influence the fluorescence intensity. The synergetic ligand TPPO with the biggest volume, could effectively shield the excited Eu^{3+} from deleterious deactivation and it almost depletes no energy compared with others, thus LB films containing Eu(TTA)$_3$(TPPO)$_2$ has the lower-energy vibrations and emits the strongest red light. Besides strongest red-light emission, more properties of LB films containing Eu(TTA)$_3$(TPPO)$_2$ will be discussed later in a separate part.

The relative intensity ratio R of $^5D_0 \rightarrow {}^7F_2$ to $^5D_0 \rightarrow {}^7F_1$ transition is commonly used to measure the local symmetry of Eu^{3+} [27,28] and is also used as monochromacity factor [22]. Increasing the local symmetry of Eu^{3+} will lead a smaller R [$R = I(^5D_0 \rightarrow {}^7F_2)/I(^5D_0 \rightarrow {}^7F_1)$]. The value of R was also used to describe the forming process and the supermolecular structures of LB films [22].

R values of AA/Eu(TTA)$_3$nL (AA:Eu = 1:1) LB films were calculated in terms of the spectra in Fig. 2 and are listed in Table 1. The results show that the bigger the volume of the synergetic ligands is, the bigger R is. It is known from experiment part that LB films were fabricated at a high surface pressure

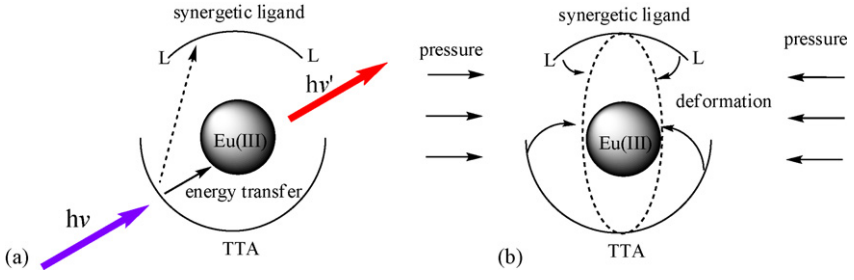

Fig. 3. (a) Process of light absorption, energy transfer and light emission of rare earth complex. (b) Process of deformation of rare earth complex under pressure.

Table 1
The value R of AA/ $Eu(TTA)_3nL = 1/1$ LB films which were deposited at 30 mN/m

LB films	R
$AA/Eu(TTA)_3(TPPO)_2 = 1/1$ LB film	10.4
$AA/Eu(TTA)_3Phen = 1/1$ LB film	6.4
$AA/Eu(TTA)_3Bipy = 1/1$ LB film	6.4
$AA/Eu(TTA)_3{\cdot}2H_2O = 1/1$ LB film	2.1

(30 mN/m). Under this circumstance, the barrier would compress the film at the air/subphase interface and the ligands would deform (see Fig. 3b). Because the volume of TPPO is much bigger than H_2O, the degree of deformation of $Eu(TTA)_3(TPPO)_2$ would be much more than that of $Eu(TTA)_3{\cdot}2H_2O$, which results that R value of $Eu(TTA)_3(TPPO)_2$ is much bigger than that of $Eu(TTA)_3{\cdot}2H_2O$. Further more, from this point, it is easily to deduce that R values of LB films containing $Eu(TTA)_3Phen$ and $Eu(TTA)_3Bipy$ would be between R values of LB films containing $Eu(TTA)_3(TPPO)_2$ and $Eu(TTA)_3{\cdot}2H_2O$, because the volume of Phen and Bipy were between TPPO and H_2O. From Table 1, the result is identical with such a deduction. On the other hand, it is also shown in Table 1 that R values of $AA/Eu(TTA)_3Phen$ and $AA/Eu(TTA)_3Bipy$ are both 6.4. This result is quite strange at first thinking, because R values of $Eu(TTA)_3Phen$ and $Eu(TTA)_3Bipy$ is different in other systems (for example, in $Eu(TTA)_3nL$ doped PMMA [9] and in solution). Therefore, this character must have something to do with the special structure of the LB films, and further discussion is given in the next part.

3.2. Model for supermolecular structure of LB films containing rare earth complexes

In this part, miscibility of AA and $Eu(TTA)_3nL$ were studied by measuring π–A isotherms with different amount of $Eu(TTA)_3nL$ for each LB film, not only because it is needed to explain the unique phenomenon mentioned above, but also because miscibility is very important for the mechanical properties and applications of LB films.

Fig. 4 shows four typical π–A (π is the surface pressure and A is the average molecular area) isotherms of mixed AA and $Eu(TTA)_3nL$ with $X_{AA} = 50\%$ (molar fraction of AA). The complexes could be divided into two classes according to the π–A isotherms. Complexes with the synergetic ligands Bipy, TPPO and H_2O belong to Class 1, the π–A isotherms of them have only one collapse pressure, indicating that the complexes are mixed well with AA, and no phase separation occurs. Complex with the synergetic ligand Phen belongs to Class 2. Its π–A isotherm has two collapse pressure. It is known that the collapse pressure of the mixed films is a good indication of the miscibility of the mixed system [29]. Two collapse pressures indicated that phase separation occurred during compression and one collapse pressure means good miscibility of the two compositions. Form the two collapse pressures as shown by curve a in Fig. 4, $Eu(TTA)_3Phen$ is first squeezed out to form its own domains, which can be further explained by experiment on limiting areas as a function of complex contents as shown in Fig. 5 (the relationship of the limiting area (A_{lim}) of the first collapse and the molar fraction of $Eu(TTA)_3Phen$ (X_{Eu})). A linear relationship can be found between A_{lim} and X_{Eu}. When $X_{Eu} = 1$, $A_{lim} = 1.26\ nm^2$, which is associated with the molecule area of $Eu(TTA)_3Phen$ and identical with the result for the molecule area of the rare earth complexes obtained by MM2-optimized model [30]. When $X_{Eu} = 0.5$, a monolayer, composed of $Eu(TTA)_3Phen$ and AA, was formed at $A_{lim} = 0.66\ nm^2$. With the pressure increasing during compressing, the first collapse was taken place due to the collapse of the $Eu(TTA)_3Phen$ monolayer, and $Eu(TTA)_3Phen$ was squeezed out to form its own domains. In Zhang et al. [30], the structure of mixed Langmuir films of stearic acid/$Eu(TTA)_3Phen$ was studied, similar results were observed under fluorescence microscope and scanning force microscopy (SFM).

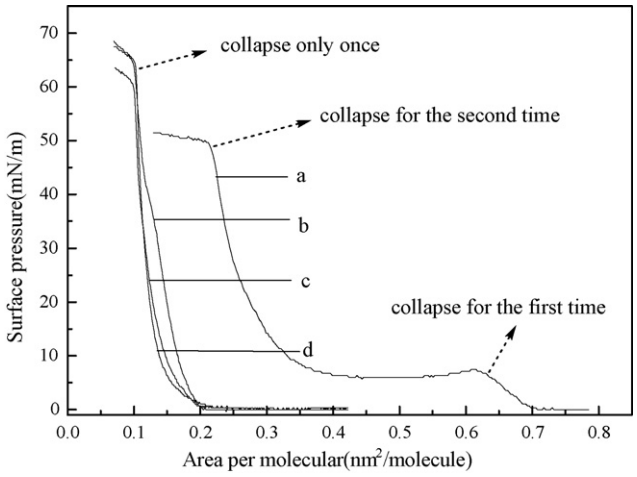

Fig. 4. The π–A isotherms with the molar fraction of X_{AA}:$X_{Eu} = 1{:}1$, (a) $AA/Eu(TTA)_3Phen$, (b) $AA/Eu(TTA)_3Bipy$, (c) $AA/Eu(TTA)_3(TPPO)_2$ and (d) $AA/Eu(TTA)_3{\cdot}2H_2O$.

π–A isotherms of $AA/Eu(TTA)_3nL$ with different molar fraction were also measured as a function of X_{AA} by using the same method used in our previous work [31], from which relationship

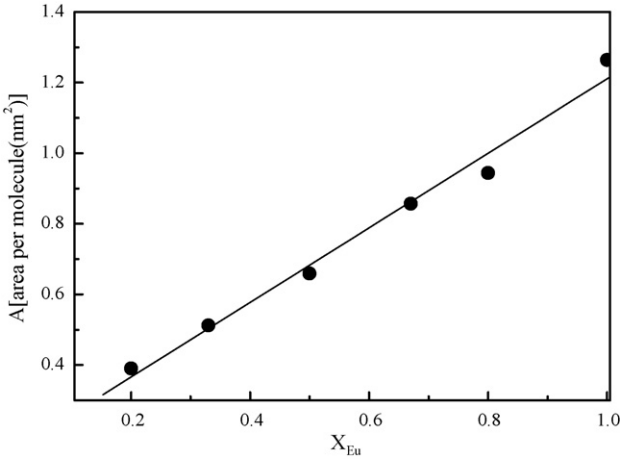

Fig. 5. Limiting areas (first collapse, ±2%) of mixed films of $AA/Eu(TTA)_3Phen$ as a function of X_{Eu}.

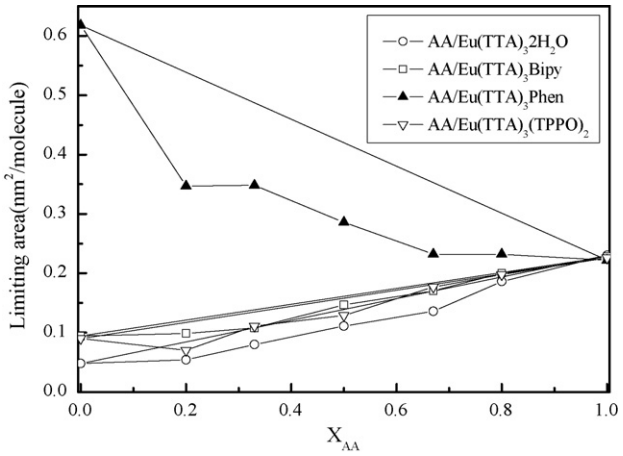

Fig. 6. Limiting areas (±2%) of AA, Eu(TTA)$_3$nL,mixed films of AA/Eu(TTA)$_3$nL at air/subphase interface as a function of X_{AA}.

of limiting areas and X_{AA} (Fig. 6) and compressibility and X_{AA} (Fig. 7) can be obtained, and more difference between the two classes of mixed films can be found in Figs. 6 and 7.

Fig. 6 shows the limiting areas (for AA/Eu(TTA)$_3$Phen, it is the limiting area of the second collapse, different from the result in Fig. 5) as a function of the molar fraction(X_{AA}) of the mixture. When $X_{AA} = 0$, it can be seen that each limiting area (calculated from the π–A isotherms) of complexes is much smaller than the molecule area of the complex (about 1.2 nm^2/molecule). There are two possible factors for such a difference in limiting areas: one comes from multilayer structure that will result in smaller A_{lim} and another from aggregate structure that results in larger A_{lim}. In multilayer structure, each molecule as a unit arranged at the air/subphase interface, it is rather condensed, but in aggregate structure, each aggregate as a unit arranged at the air/subphase interface, there must be some "interstices" among the aggregates, because an aggregate is not as regular as a rare earth complex molecule. The result shown in Fig. 6 indicates that AA/Eu(TTA)$_3$Phen Langmuir films have bigger A_{lim}, so aggregates was formed; other LB films have smaller A_{lim}, multilayer structure formed. On the other hand, it can be seen in Fig. 6 that AA/Eu(TTA)$_3$Phen Langmuir films have bigger negative deviation (compared with its own theoretical result for an ideal binary mixed layer) than that of other systems, by which the conclusion above can be further conformed because there are some "interstices" among the aggregates, AA can occupy these "interstices", and there will be a bigger negative deviation when aggregates formed; in multilayer structure, it is quite condensed, there will be only very small negative deviation because of the attracting of the AA and the complexes [31]. It can also be found in Fig. 6 that the limiting areas of AA/Eu(TTA)$_3$Phen increases with the decreasing of X_{AA} and the limiting areas of AA/Eu(TTA)$_3$nL (L = TPPO, Bipy, H_2O) increases. This is because the area occupied by the aggregate is bigger than AA, and the area occupied by the multilayer is smaller than AA. Further explain can be obtained by detailed analysis of the slope of isotherms given below.

The compressibility modulus of a film can be calculated according to the formula $E_0 = -A(d\pi/dA)$, where E_0 is compressibility modulus. For an ideal binary mixed monolayer, its

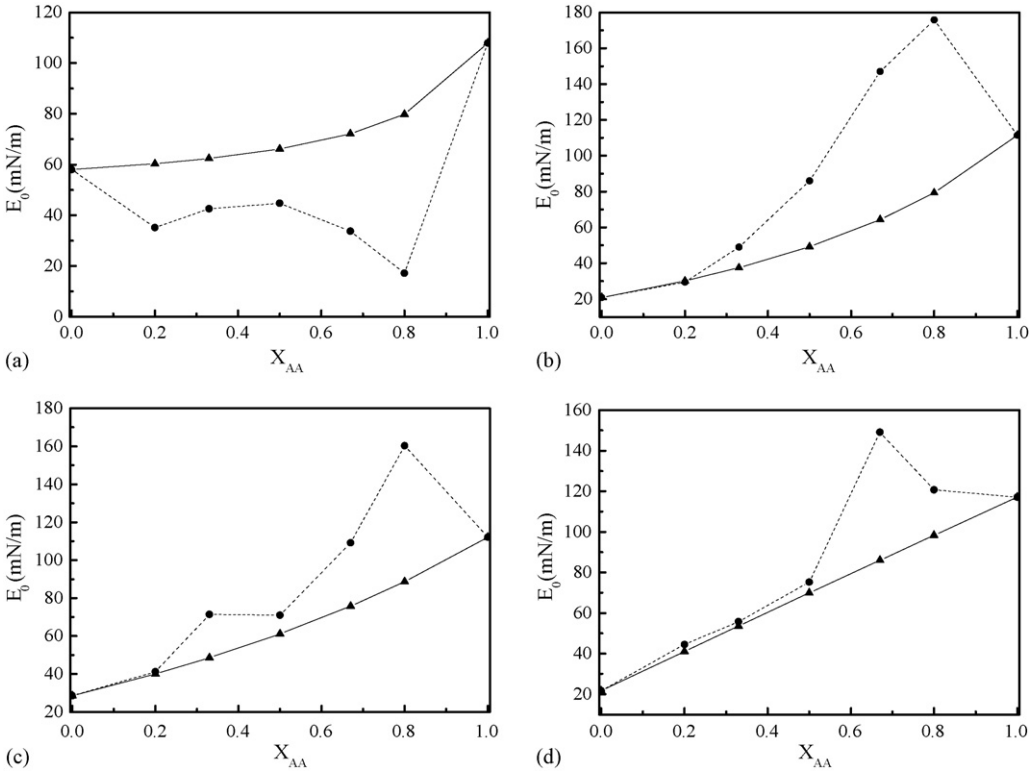

Fig. 7. (●) E_0(±2%) and (▲) E^{id} of AA, Eu(TTA)$_3$nL, mixed films of AA/Eu(TTA)$_3$nL at the air/subphase interface as a function of X_{AA} at the surface pressure 12 mN/m. (a) AA/Eu(TTA)$_3$Phen, (b) AA/Eu(TTA)$_3$Bipy, (c) AA/Eu(TTA)$_3$(TPPO)$_2$ and (d) AA/Eu(TTA)$_3$·2H$_2$O.

compressibility modulus (E^{id}) can be easily derived by applying the equation $A_{12} = X_1A_1 + X_2A_2$ (A_1, A_2, A_{12} represent the molecular area of monolayer of each component and their mixture, respectively; X_1, X_2 represent the molar fraction of each component), and is given by: $E^{id} = A_{12}E_1E_2/(X_1A_1E_2 + X_2A_2E_1)$, where $E_1 = -A_1(d\pi/dA_1)$ and $E_2 = -A_2(d\pi/dA_2)$ are the compressibility modulus of the individual monolayer, respectively. This value is particularly interesting for the description of the film phase behavior and for investigating the miscibility of two pure components in the mixed film at the air/subphase interface [31–33]. In Fig. 7, the values of E_0 and E^{id} are shown for LB films containing each rare earth complex, from which E_0 of the mixed films AA/Eu(TTA)$_3$Phen had negative deviations to E^{id}, and E_0 of the other three systems had positive deviations to E^{id}. A negative deviation (AA/Eu(TTA)$_3$Phen system) means the film-forming molecules have repulsive interactions at the air/subphase interface, and phase separation took place. A positive deviation (the other three systems) means the mixed films are more compressible than the idea compression of the pure component's films, two components of the mixed films must mixed well and have attractive interactions at the air/subphase interface.

From what had been discussed above, possible supermolecular structures of AA/Eu(TTA)$_3$nL were proposed as shown in Fig. 8. In Fig. 8a, the model of AA/Eu(TTA)$_3$Phen phase change at the air/subphase is shown. State (I) is a classical "gas" film, there is no increment of the surface pressure. As the barrier compresses the film, the surface pressure begins to increase at a point, phase change occurred. From Fig. 5, it is known that state (II) is the process of forming Eu(TTA)$_3$Phen monolayer. When the surface pressure reaches a maximum (about 8 mN/m), the film collapsed, it is the collapse of Eu(TTA)$_3$Phen monolayer. Eu(TTA)$_3$Phen was squeezed out to form aggregates. As the barrier compresses the film, surface pressure has a rapid increment. The film is compressed to a condensed "solid" state. That is the state (III).

In Fig. 8b, the model of AA/Eu(TTA)$_3$nL (L = Bipy, H_2O, TPPO) is shown. This model is similar to the model in our previous work [34] when rare earth complexes have good miscibility with AA. State (I) is also a classical "gas" film. State (II) is a classical "liquid" film. The film forming molecules begin to pack together. State (III) is the state of the "solid" film. The slope is bigger and did not change in this state. It is a very condensed state. AA keeps its monolayer state (see Fig. 10) and rare earth complexes formed multilayer.

According to the model above, it is easier now to understand that complexes with different synergetic ligands Phen and Bipy have the same R values (as shown in Table 1). Because the volume of Phen is larger than that of Bipy, R value of Eu(TTA)$_3$Phen is larger than that of Eu(TTA)$_3$Bipy in solid system [10]. However, in LB film system, due to the supermolecular structures, Eu(TTA)$_3$Bipy is mixed well with AA and has a small limiting area compared with Eu(TTA)$_3$Phen in aggregates. Under this circumstance, the degree of deformation of Eu(TTA)$_3$Bipy would be more than that of Eu(TTA)$_3$Phen, which would result in increasing of R value. If we consider both the molecular structure and the supermolecular structure of AA/Eu(TTA)$_3$Phen and AA/Eu(TTA)$_3$Bipy, the same R values of them is understandable. This fact reveals that R could be affected by both of the volume of the ligand (molecular structure) and the supermolecular structures.

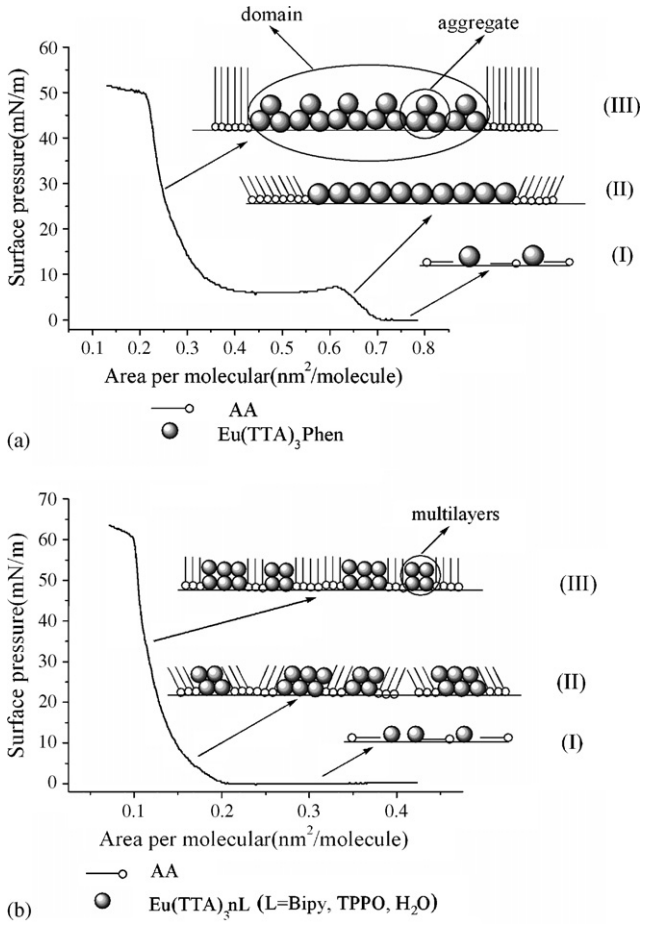

Fig. 8. Possible supermolecular structures of AA/Eu(TTA)$_3$nL mixed films at the air/subphase interface (a) AA/Eu(TTA)$_3$Phen and (b) AA/Eu(TTA)$_3$nL (L = Bipy, TPPO, H_2O).

3.3. Fluorescence of AA/Eu(TTA)$_3$(TPPO)$_2$ LB film

Eu(TTA)$_3$(TPPO)$_2$ doped PMMA has been found to have the longest radiative time compared to complexes with other synergetic ligands [10]. In LB film system, it is also found it have the strongest emission as shown in Fig. 2. In this part, relationship between fluorescence and supermolecular structure of AA/Eu(TTA)$_3$(TPPO)$_2$ LB film is discussed.

The UV–vis spectra of Eu(TTA)$_3$(TPPO)$_2$ in $CHCl_3$ solution and AA/Eu(TTA)$_3$(TPPO)$_2$ LB film are shown in Fig. 9. Strong absorption bands according to the $\pi \rightarrow \pi^*$ transition of the ligands of Eu(TTA)$_3$(TPPO)$_2$ can be observed. The complex exhibits a UV absorption peak at 341 nm in $CHCl_3$ solution, which is red-shifted to 359 nm in LB film. The UV spectral differences observed between the solution and the LB film indicate that the complex have a highly ordered arrangement in the film [35,36] and the complex has a strong interaction with AA [31]. The red-shift of UV absorption peak of Eu(TTA)$_3$Phen in LB films to $CHCl_3$ solution is only 3 nm

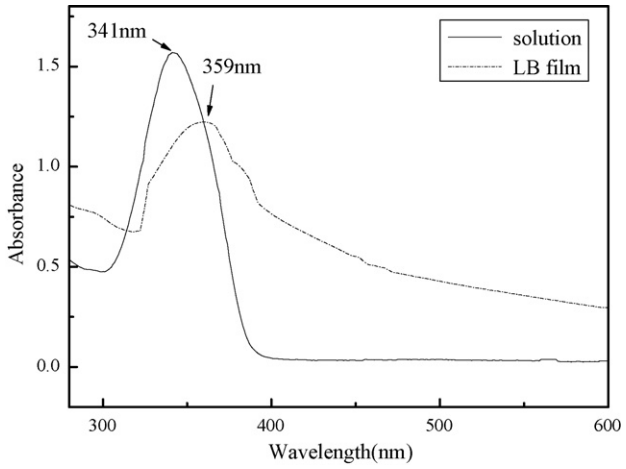

Fig. 9. UV–vis spectra of $Eu(TTA)_3(TPPO)_2$ $CHCl_3$ solution and AA/$Eu(TTA)_3$ $(TPPO)_2$ LB film.

(see supplementary materials, Fig. S1), which indicates that the interaction between AA and $Eu(TTA)_3Phen$ is weaker than that of AA and $Eu(TTA)_3(TPPO)_2$. This result is accordance with the result obtained from the film supermolecular structure study at the air/subphase interface: $Eu(TTA)_3(TPPO)_2$ mixes well with AA, and $Eu(TTA)_3Phen$ not, there is phase separation between $Eu(TTA)_3Phen$ and AA, so the interaction of AA and $Eu(TTA)_3Phen$ is weaker.

Small angle X-ray diffraction pattern of a 26-layer AA/$Eu(TTA)_3(TPPO)_2$ LB film is shown in Fig. 10. Several Bragg diffraction peaks can be observed in the range $2\theta = 1–10^\circ$ indicating the presence of a regular, periodic structure in the LB film. The identity period of the LB film can be expressed as $d = ld_{001}$. From this equation, the identity period of the LB film is calculated to be $d = 5.47$ nm, which is comparable to the well-known fatty acid salt LB films. This result reveals that AA can be used to control the film thickness at nanometer-scale very well.

Fluorescence spectroscopy of the AA/$Eu(TTA)_3(TPPO)_2$ LB films in different number of layers is shown in Fig. 11.

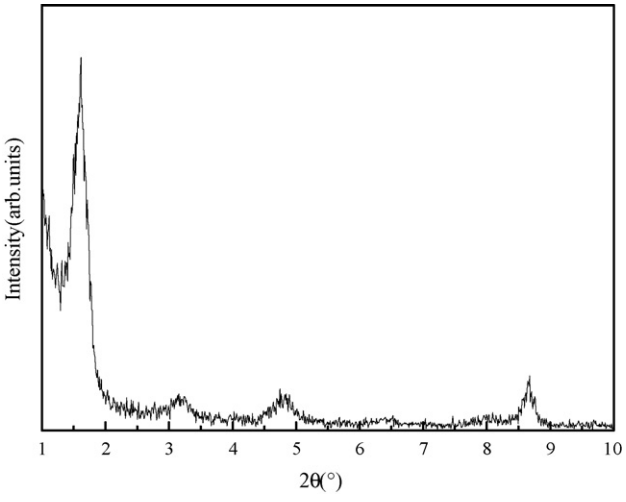

Fig. 10. Small angle X-ray diffraction pattern of 26-layer AA/$Eu(TTA)_3$ $(TPPO)_2$ LB film.

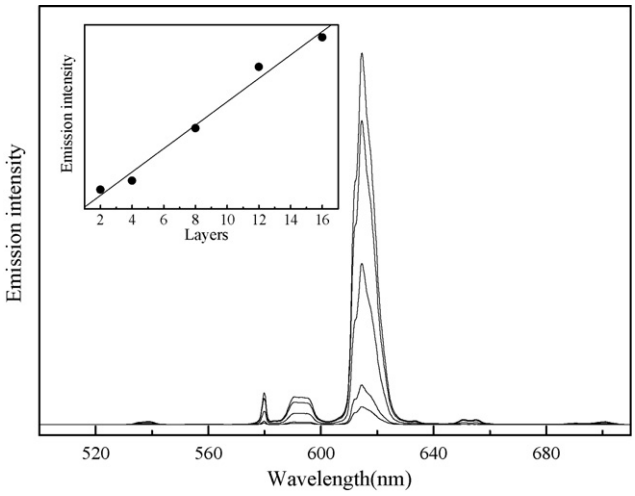

Fig. 11. Fluorescence spectra of AA/$Eu(TTA)_3(TPPO)_2$ = 1/1 LB films in different number of layers. The inset is the plot of the emission intensity of $^5D_0 \rightarrow {}^7F_2$ vs. the number of layers.

When the number of layers increasing, the emission intensity also increased. The linear relationship between emission intensity of $^5D_0 \rightarrow {}^7F_2$ (peak around 615 nm) and the number of layers is directly resulted from the successive and regular deposition of AA/$Eu(TTA)_3(TPPO)_2$ LB films. This means that $Eu(TTA)_3(TPPO)_2$ does not only mix well with AA in the Langmuir monolayer but also has a vertical uniformity in the LB films. It also indicates that there is no aggregate structure between layers and no quenching effect of the fluorescence, which would directly result in that the fluorescence intensity of the films could be modulated by depositing different number of layers. All these characteristics are good enough to allow AA/$Eu(TTA)_3(TPPO)_2$ LB films to make into high quality optical devices.

4. Conclusion

In this paper, Langmuir and Langmuir–Blodgett films containing four europium complexes with different synergetic ligands are studied. The fluorescence enhancement of rare earth complexes in the LB films resulted from synergetic ligands was observed for the first time. A parameter R is discussed in detail. Through film behavior study, it is found the π–A isotherms' shapes, forms of collapse, limiting areas, and compressibility modulus of $Eu(TTA)_3Phen$ containing LB films are different from those of the other three europium complexes. It indicates that the aggregate supermolecular structure is formed in LB film containing $Eu(TTA)_3Phen$, and multilayer structure in LB films containing other three europium complexes. The degree of deformation of $Eu(TTA)_3Bipy$ is more than that of $Eu(TTA)_3Phen$ within LB films, which results in unique increasing of R value of $Eu(TTA)_3Bipy$. AA/$Eu(TTA)_3(TPPO)_2$ LB films is found not only to have the strongest red light emission, the best monochromacity, good miscibility with AA but also have condensed structure, controllable nanometer-scale thickness and vertical uniformity which allow it to be used as high quality ultrathin optical devices.

Acknowledgments

This work is supported by the National Natural Science Foundation of China (Grant Nos. 50533040 and 50573071) and National Basic Research Program of China (No. 2006cb302900).

Appendix A. Supplementary data

Supplementary data associated with this article can be found, in the online version, at doi:10.1016/j.jphotochem.2006.12.020.

References

[1] V. Bekiari, P. Lianos, Adv. Mater. 10 (1998) 1455.
[2] J. Kido, H. Hayase, K. Hongawa, K. Nagai, Appl. Phys. Lett. 65 (1994) 2124.
[3] F.S. Richardon, Chem. Rev. 82 (1982) 541.
[4] O. Prat, E. Lopez, G. Mathis, Anal. Biochem. 195 (1991) 283.
[5] K. Binnemans, C. Görller-Walrand, Chem. Rev. 102 (2002) 2303.
[6] Q. Zhang, P. Wang, X. Sun, Y. Zhai, P. Dai, B. Yang, H. Ming, J. Xie, Appl. Phys. Lett. 72 (1998) 407.
[7] H. Liang, Z. Zheng, Q. Zhang, H. Ming, Z. Li, J. Xu, B. Chen, H. Zhao, Optics Lett. 29 (2004) 477.
[8] H. Jiu, H. Tang, J. Zhou, J. Xu, Q. Zhang, H. Xing, W. Huang, A. Xia, Optics Lett. 30 (2005) 774.
[9] H. Liang, Z. Zheng, Q. Zhang, H. Ming, B. Chen, J. Xu, H. Zhao, J. Mater. Res. 18 (2003) 1895.
[10] J.B. Guan, B. Chen, Y.Y. Sun, H. Liang, Q.J. Zhang, J. Non-Cryst. Solids 351 (2005) 849.
[11] Y.Y. Sun, H.F. Jiu, D.G. Zhang, J.G. Gao, B. Guo, Q.J. Zhang, Chem. Phys. Lett. 410 (2005) 204.
[12] G.G. Roberts, Langmuir–Blodgett Films, Plenum Press, New York, 1990.
[13] U. Ulman, An Introduction to Ultrathin Organic Films, from Langmuir–Blodgett to Self Assembly, Academic Press, San Diego, 1991.
[14] R.H. Tredgold, Order in Thin Organic Films, Cambridge University Press, Cambridge, 1994.
[15] P. He, in: L. Shi, D. Zhu (Eds.), Polymers and Organic Solid, Science Press, Beijing, 1997, p. 25.
[16] Y. Ando, T. Hiroike, T. Miyashita, T. Miyazaki, Thin Solid Films 266 (1995) 292.
[17] T. Tippmann-Krayer, W. Meisel, U. Hohne, H. Mohwald, Makromol. Chem. Macromol. Symp. 46 (1991) 214.
[18] T. Faldum, W. Meisel, P. Guitlich, Surf. Interface Anal. 24 (1996) 68.
[19] T. Faldum, W. Meisel, P. Guitlich, Hyperfine Interact. 92 (1994) 1263.
[20] D. Brandl, Ch. Schoppmann, Ch. Tomaschko, J. Markl, H. Voit, Thin Solid Films 249 (1994) 113.
[21] D.T. Amm, D.J. Johnson, T. Laursen, S.K. Gupta, Appl. Phys. Lett. 61 (1992) 522.
[22] K.Z. Wang, L.H. Gao, C.H. Huang, J. Photochem. Photobiol. A-Chem. 156 (2003) 39–43.
[23] P.S. He, G. Zou, K. Fang, Acta Phys. Chim. Sin. 20 (2004) 1275.
[24] T. Cardinaels, K. Driesen, N. Tatjana, B. Parac-Vogt, C. Heinrich, D. Bourgogne, B. Guillon, K. Donnio, Binnemans, Chem. Mater. 17 (2005) 6589.
[25] P. Lenaerts, A. Storms, J. Mullens, J. D'Haen, C. Görller-Walrand, K. Binnemans, K. Driesen, Chem. Mater. 17 (2005) 5194.
[26] R.J. Zhang, K.Z. Yang, Colloids Surf. A 178 (2001) 177.
[27] E.B. Stucchi, S.L. Scapari, M.A. Coutodossantos, S.R.A. Leite, J. Alloys Compd. 275 (1988) 89.
[28] Y. Nageno, H. Takebe, K. Morinaga, T. Izumitani, J. Non-Cryst. Solids 169 (1994) 288.
[29] L. Gaines Jr., Insoluble Films at Liquid–Gas Interfaces, Interscience, New York, 1976.
[30] R.J. Zhang, P. Krüger, B. Kohlstrunk, M. Lösche, ChemPhysChem 2 (7) (2001) 452.
[31] G. Zou, K. Fang, P.S. He, J. Colloid Interface Sci. 261 (2003) 411.
[32] G.L. Gaines Jr., Insoluble Monolayers al Liquid–Gas Interfaces, Interscience Publishers, New York, 1966.
[33] P.S. He, K. Fang, G. Zou, J.P.K. Peltonen, J.B. Rosenholm, Colloids Surf. A 201 (2002) 265.
[34] G. Zou, Y.Z. Zhang, P.S. He, Thin Solid Films 468 (2004) 268.
[35] R.J. Zhang, K.Z. Yang, Langmuir 13 (1997) 7141.
[36] G.L. Zhong, K.Z. Yang, Langmuir 14 (1998) 5502.